frontiers | Frontiers in Energy Research

ORIGINAL RESEARCH
published: 08 June 2022
doi: 10.3389/fenrg.2022.914291

A Comparative Study of SOC Estimation Based on Equivalent Circuit Models

Jiangtao He[1], *Shujuan Meng*[1]* *and Fengjun Yan*[2]

[1]School of Space and Environment, Beihang University, Beijing, China, [2]Department of Mechanical Engineering, McMaster University, Hamilton, ON, Canada

This article presents a comparative study of the state of charge (SOC) estimation using Kalman filter (KF)-based estimators and H-infinity filter. The aim of this research is to obtain the optimal estimator by evaluating the SOC accuracy, robustness, and computation time under varying current noise assumptions. In the KF-based estimators, the extended Kalman filter (EKF), unscented Kalman filter (UKF), and cubature Kalman filter (CKF) are mostly used in the SOC estimation area. The mixed driving cycle profiles are used to test the battery to simulate the complex driving conditions in real electric vehicles (EVs). Also, white noise and bias noise are added into the current data to imitate the inaccurate sensors in EVs. The normal equivalent circuit models (ECMs) and augmented ECMs with varying RC branches are thoroughly compared to acquire the best estimator under varying situations.

Keywords: state of charge, equivalent circuit model, state estimation, H-infinity, lithium-ion (Li^+) batteries

OPEN ACCESS

Edited by:
Yujie Wang,
University of Science and Technology of China, China

Reviewed by:
Yang Li,
Chalmers University of Technology, Sweden
Binyu Xiong,
Wuhan University of Technology, China
Kailong Liu,
University of Warwick, United Kingdom

***Correspondence:**
Shujuan Meng
mengsj@buaa.edu.cn

Specialty section:
This article was submitted to Electrochemical Energy Conversion and Storage, a section of the journal Frontiers in Energy Research

Received: *06 April 2022*
Accepted: *26 April 2022*
Published: *08 June 2022*

Citation:
He J, Meng S and Yan F (2022) A Comparative Study of SOC Estimation Based on Equivalent Circuit Models. Front. Energy Res. 10:914291. doi: 10.3389/fenrg.2022.914291

1 INTRODUCTION

The state of charge (SOC) is defined as the ratio of $C_{remain}/C_{available}$ for a battery cell or a battery pack (Wang et al., 2020). In EVs, the SOC of the battery pack is similar to the fuel gauge of gasoline vehicles, except that the SOC is not directly measurable (Liu et al., 2022a). So, first, the accurate SOC is eagerly needed by the customers who drive the EVs in a variety of operating conditions (such as highway, local, or traffic jams) to avoid being stuck on the way. Second, accurate SOC is helpful to manage the battery pack, such as draining out the energy stored in the pack while not damaging the battery for over-discharging, running cell balancing, and state of health (SOH) estimation (Wei et al., 2021a). Lastly, accurate SOC will save the cost of the battery pack since extra battery cells are not needed to make sure the EVs reach a specific range (such as the Tesla Model S 90D, range: 473 km) since the accurate SOC could guarantee the battery pack's full discharge without damaging it.

In brief, the SOC is a critical parameter to the battery management system (BMS) in EVs; since it cannot be obtained through a sensor test, a variety of methods have been proposed to estimate the SOC (Wei et al., 2021b). Cuma and Koroglu (2015) categorized the existing SOC estimation methodologies into five groups, as shown in **Figure 1**. All the acronyms in **Figure 1** could be found in the nomenclature table in the article. The conventional and adaptive filter algorithms are the focus of this paper since they are easily implemented with relatively high SOC accuracy and reasonable computation requirements (Wei et al., 2017). In the industrial field, the Ampere-Hour integral (coulomb counting) method is still used to acquire the SOC, although it will accumulate the SOC error and the accuracy is highly dependent on the sensor accuracy level (Lu et al., 2013). To enhance the SOC accuracy, Yang et al. (2015) proposed a revised coulomb counting method which can capture the dynamic responses of SOC during the pulse discharge operations by correlating the

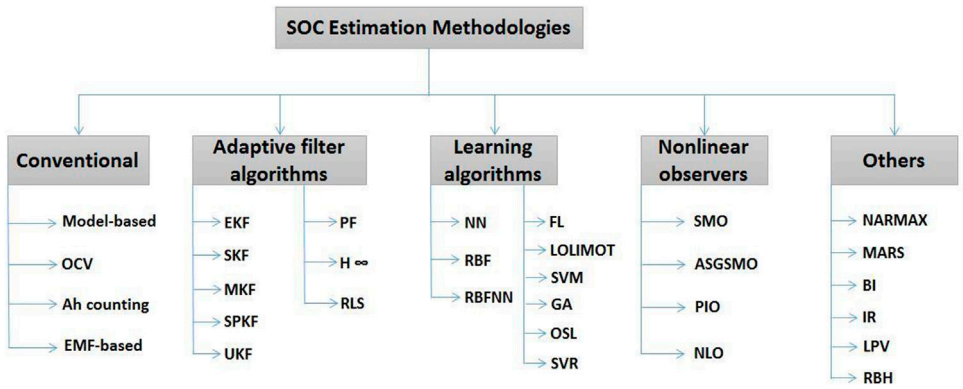

FIGURE 1 | Categorization of SOC estimation methodologies.

available capacity with the amount of dischargeable lithium ion in the electrode particles. The other option is combining the open circuit voltage (OCV) method with the ECM to estimate the SOC based on estimators (such as EKF, SVSF, and H-infinity). Also, for model-based methods, the other main part is the electrochemical model (Li et al., 2021; Liu et al., 2022b). Ahmed et al. (2014) proposed a reduced-order electrochemical model to estimate the SOC considering the aging effect. Although the model is highly simplified, there are still 18 parameters that need to be identified, which could cause high computation effort.

For the ECM model, it only uses electrical components, such as resistors and capacitors, to model the electrochemical physics of a lithium ion battery, to estimate the SOC accurately, identified battery model parameters and proper filters are needed to deal with the noise (Wei et al., 2018). Since the noise is unknown information, the ability to filter the noise will have an effect on the estimated SOC accuracy (Wei et al., 2020a). For instance, the Kalman filter-based estimators assume the noise is white Gaussian form. Plett (2004) in his series of papers proposed a mathematical model including terms that describe the dynamic contributions due to OCV, ohmic loss, polarization time constants, electrochemical hysteresis effect, and temperature effect to estimate the SOC using EKF. Xiong et al. (2013a) used the adaptive EKF to estimate the battery pack's SOC with 2% SOC error by regarding the battery pack model as a unit battery cell model. Sun et al. (2011) presented an AUKF to estimate the SOC by adaptively adjusting the noise covariances. Compared with AEKF, the UKF-based algorithm shows better accuracy in SOC estimation. Xia et al. (2015) propose an ACKF-based SOC estimator for lithium ion batteries in EVs, which shows better performance in estimated SOC accuracy, convergence speed, and robustness against voltage measurement noise compared with EKF and CKF algorithms. Nevertheless, the estimated SOC accuracy may decrease when the process noise and the measurement noise are uncorrelated with zero mean Gaussian white noise, especially when the cell's battery model is scaled up to estimate the battery pack's SOC (Wei et al., 2022a). To deal with the estimators' robustness, a SVSF estimator based on a sliding mode observer and an H-infinity filter is proposed to estimate the SOC. Kim et al. (2014) used the iterated SVSF to perform the SOC estimation, which shows the application potential for real-time embedded BMS due to its low complexity, high accuracy, and robustness. Since the H-infinity filter was specially designed for robustness, which means it can still guarantee the SOC estimation accuracy even if no assumptions about the statistics of the process and measurement noise are made. Zhang et al. (2012) used the H-infinity observer to estimate the battery SOC under different current and temperature operating conditions, the estimated SOC errors increase with larger current, while it is still less than 2%, also, the SOC accuracy is less than 2% at different operating temperatures. Wei et al. (2021c) and Wei et al. (2022b) proposed a model-based current-unknown SOC estimator based on the moving horizon observation theory. Results suggested that the SOC was estimated with high accuracy even if the current of the battery was not available.

From the literature review, all estimators based on equivalent circuit models are claimed to have high accuracy and robustness to estimate the SOC. In this paper, these estimators will be evaluated by examining their estimation error, robustness, sensitivity to noise, and computational time. Also, it is worth mentioning that many of the SOC papers use the same current data to calculate the "actual" SOC (reference SOC) and to obtain the estimated SOC by using the current data as input to the ECM-based estimators. Here, the only function of these estimators is to minimize the error of the inaccurate preset initial SOC value and to filter the noise caused by the inaccurate ECM model. However, in real EVs, the current sensors may have some bias noise, which is difficult for the KF based estimators to fully remove it. In this paper, the augmented ECM (the idea comes from Dr. Daiwei Feng) is proposed to handle the bias noise and guarantee that the estimators are convergent.

The remainder of this paper is organized as follows. The experimental setup to obtain the data is described in **Section 2**. The basic knowledge about the SOC estimation, which includes the ECM model, parameters identification methods, and hysteresis effect are described in **Section 3**. The key features for implementing the four estimators (EKF, UKF, CKF, and H-infinity) are described in **Section 4**. The estimators'

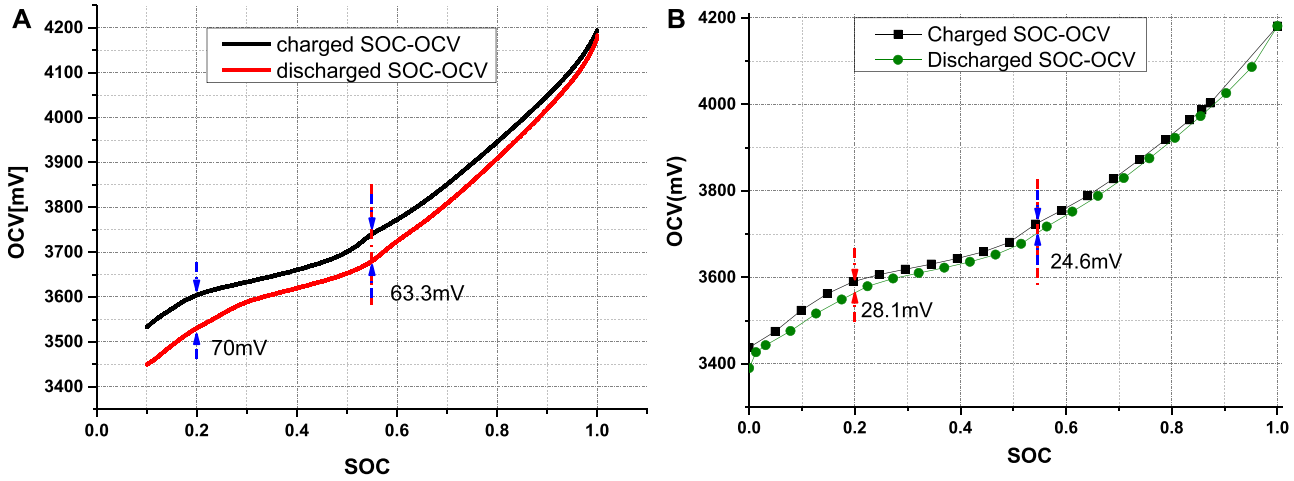

FIGURE 2 | (A) OCV-SOC curve using method A (10–100% SOC); **(B)** OCV-SOC curve-method B (0–100%).

comparison results are discussed in **Section 5**, followed by conclusions presented in **Section 6**.

2 BATTERY TEST EXPERIMENTS

The current and voltage data used in this study are tested by the Arbin BT 2000 (sensors' accuracy 0.1%) and a thermal chamber. The tested cylindrical Li-ion cells (LiNMC) with a nominal capacity of 2.2 A h are from Xi'an New Energy. Since the computation time of the estimators are compared in this study, the MATLAB 2014a is used in the computer with Intel®Core ™ i7 processor 4,790 to run the simulation.

In order to build the ECM model and to demonstrate the performance of the proposed estimators, the following tests were selected for the study.

a. OCV-SOC relationship

This test is used to obtain the open circuit voltage (OCV)-SOC relationship. This test is important since the OCV (soc) function in the ECM is obtained by fitting the OCV-SOC curve. In the literature, very small C-rates (C/20) (Wei et al., 2021b), hybrid pulse power characterization (HPPC) (U.S. Department of Energy, 2001), and 0.5C-rate charge/discharge with 1 h relaxation at 5% SOC interval are three of the most commonly used methods to obtain the OCV-SOC curves. However, which one is the best? In order to compare the C/20-rate charge/discharge (Method A) and 0.5C-rate charge/discharge with 1 h of rest (Method B), the same battery was tested at ambient temperature, as shown in **Figure 2A, B**. From **Figure 2**, the SOC error at 20%SOC and 55% SOC is 70 and 63.3 mV for Method A, and 28.1 and 24.6 mV for Method B. The other 10 cells' results are shown in **Table 1**. The mean values of Method A at 20% and 55%SOC are 72.5 mV and 59.7 mV, respectively, while the mean values of Method B are 25.6 mV and 20.4 mV, respectively. The results show that Method B to obtain the OCV-SOC curves is more accurate than Method A. The HPPC only has discharged OCV-SOC curves, so it is not involved in the comparison. Even though the HPPC test is not used to obtain the OCV-SOC curves in this study, it is still needed to identify the model parameters.

b. UDDS and mixed driving cycle tests

To generate the current profiles needed for battery testing, an electric vehicle model in the GT-SUITE 7.4 has been modified under varying velocity profiles. The battery pack current profiles have been scaled down to the cell level for validation purposes. In this study, the urban dynamometer driving schedule (UDDS) and mixed driving cycles

$$\text{NYCC} + 2\text{UDDS} + 2\text{US06} + 2\text{LA92} + 2\text{HWY} + \text{UDDS} + 1\text{h rest} + 2\text{UDDS} + 2\text{US06} + 2\text{LA92} + 2\text{UDDS}$$

are composed to simulate the real EV's driving conditions. In the mixed current profiles, the New York City Cycle (NYCC) features low-speed stop-and-go traffic conditions. The UDDS represents the city driving conditions. The US06 is a high-acceleration, aggressive driving schedule. Compared to the UDDS, the LA92 dynamometer driving schedule has a higher top speed, a higher average speed, less idle time, fewer stops per mile, and a higher maximum rate of acceleration. The HWY represents a highway driving condition.

3 ECM-BASED SOC ESTIMATION

3.1 The Normal 2RC-ECM and Augmented 2RC-ECM

In the literature about the equivalent circuit model, the normal form of 2RC-ECM can be represented as follows (Wei et al., 2020b):

TABLE 1 | Voltage error between Method A and Method B.

Cell no.	0.02C-rate charge/discharge		0.5C-rate charge/discharge 1 h rest	
	Voltage error (mV) 20%	Voltage error (mV) 55%	Voltage error (mV) 20%	Voltage error (mV) 55%
1	70	63.3	28.1	24.6
2	72.4	58.9	19.6	11.5
3	75.2	62.4	26.7	21.9
4	74.6	61	27.8	21.8
5	73.2	60.7	27.3	22.4
6	70.6	58	23.9	18.8
7	72.4	58.9	28.4	22.7
8	72.3	57.3	27.8	22.9
9	71.7	59.7	27.2	22.7
10	74.7	60.2	28	23.3
11	70.9	56.9	17.5	11.5

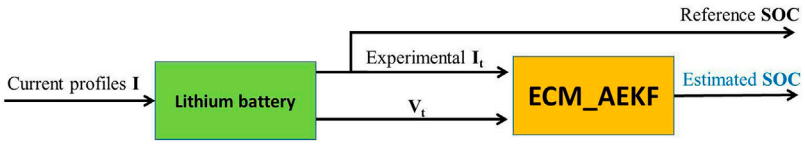

FIGURE 3 | SOC estimation strategy without sensors' noise assumption.

$$x = \left[V_{1,k+1} \quad V_{2,\,k+1} \quad Z_{k+1} \right]^T, \tag{1}$$

$$x_{k+1} = Ax_k + Bi_k + w_k \tag{2}$$

$$y_k = OCV\,(z_k) - V_{1,k} - V_{2,k} - R_0 i_k + v_k \tag{3}$$

$$A = \begin{bmatrix} exp\left(-\frac{\Delta t}{R_1 C_1}\right) & 0 & 0 \\ 0 & exp\left(-\frac{\Delta t}{R_2 C_2}\right) & 0 \\ 0 & 0 & 1 \end{bmatrix} \tag{4}$$

$$B = \begin{bmatrix} \left(1 - \exp\left(-\frac{\Delta t}{R_1 C_1}\right)\right) * R1 \\ \left(1 - \exp\left(-\frac{\Delta t}{R_2 C_2}\right)\right) * R2 \\ -\frac{\eta_i\ \Delta t}{C_n} \end{bmatrix} \tag{5}$$

where Z_k represents the SOC, C_n is the battery nominal capacity, $V_{1,k}$ $V_{2,k}$ is a state variable and represents the voltages across the two capacitors. The state variables of the system are Z_k, $V_{1,k}$, $V_{2,k}$. The output of the model is y_k, which is the terminal voltage, the current i_k is the input. The w_k and v_k are system noise and measurement noise, respectively.

Based on the ECM model, the SOC can be estimated using the estimator as shown in **Figure 3**. Here, the AEKF could be switched with the other algorithms depending on which one is suitable (Hu et al., 2021a). In the SOC research area, the current profiles I (such as UDDS) are used to excite the battery and the experimental current $\mathbf{I_t}$ and terminal voltage $\mathbf{V_t}$ are obtained. Also, the reference SOC can be calculated by using the coulomb counting method based on the current $\mathbf{I_t}$. Then, the same current data $\mathbf{I_t}$ is used to estimate the SOC based on the ECM_AEKF estimator, which also includes the coulomb counting method as shown in **Eq. 1**. So, the function of the estimator used here is to remove the error of an inaccurate preset initial SOC value and the system noise of the battery model.

However, in real EVs, the current sensors are not as accurate as the ones used on the test bench, which means the bias noise + white noise are coupled to contaminate the test data (Hu et al., 2021b; Hu et al., 2021c; Wei et al., 2022c). For the white noise, the proposed estimators (such as KF-based) are easy to remove it, however, the challenging part is the bias noise, which will cause the estimators to diverge. So, in this paper, a novel SOC estimation strategy is proposed as shown in **Figure 4**. The white current and voltage noise I_w and V_w with 0.5 amplitude and preset current bias noise I_b are used to simulate the inaccurate current and voltage sensors in the EVs. Meanwhile, the reference SOC could be regarded as the "actual" SOC since it uses much more accurate sensors in the test bench. Then, the noise-added test current and terminal voltage are fed into the ECM_AEKF estimator to estimate the SOC. Using this strategy, both the sensors' noise and the model's inaccuracy are considered, which makes it more applicable in real EVs.

As mentioned above, the bias current noise will cause the estimator to diverge. The main reason is that current integration in the ECM will accumulate the bias error due to the nonzero integration (the numerical integration for white noise is zero).

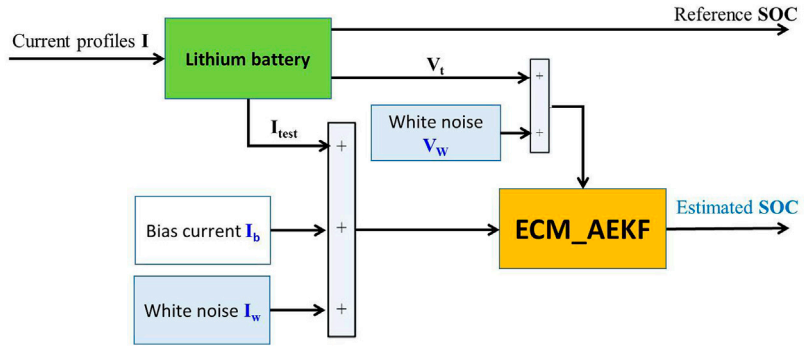

FIGURE 4 | SOC estimation strategy with sensors' noise assumption.

The augmented ECM may be a good solution to handle the bias noise by adding one more state I^b to capture the variation of the noise. Here, the 2RC augmented ECM is used for illustration purposes. Compared with the normal ECM as shown in **Equations 1**–**5**, the main differences exist in **Equations 6** and **8**, **9**, where the system and measurement equations are revised since the noise state I^b is added. It is obvious to see the noise I^b is removed from the noise added current i_k in **equation (11)**–**(13)** by multiplying the term $(i_k - I_k^b)$.

$$x = \begin{bmatrix} Z_{k+1} & V_{1,k+1} & V_{2,k+1} & I_{k+1}^b \end{bmatrix}^T \tag{6}$$

$$x_{k+1} = Ax_k + Bi_k + w_k \tag{7}$$

$$y_k = OCV(z_k) - V_{1,k} - V_{2,k} - R_0\left(i_k - I_k^b\right) + v_k \tag{8}$$

$$A = \begin{bmatrix} 1 & 0 & 0 & \frac{\eta_i \Delta t}{C_n} \\ 0 & e^{-\frac{\Delta t}{R_1 C_1}} & 0 & -R_1\left(1 - e^{-\frac{\Delta t}{R_1 C_1}}\right) \\ 0 & 0 & e^{-\frac{\Delta t}{R_2 C_2}} & -R_2\left(1 - e^{-\frac{\Delta t}{R_2 C_2}}\right) \\ 0 & 0 & 0 & 1 \end{bmatrix} \tag{9}$$

$$B = \begin{bmatrix} -\frac{\eta_i \Delta t}{C_n} & R_1\left(1 - e^{-\frac{\Delta t}{R_1 C_1}}\right) & R_2\left(1 - e^{-\frac{\Delta t}{R_2 C_2}}\right) & 0 \end{bmatrix}^T \tag{10}$$

Rewriting **Equation (7)**,

$$Z_{k+1} = Z_k - \frac{\eta_i \Delta t}{C_n}\left(i_k - I_k^b\right), \tag{11}$$

$$V_{1,k+1} = e^{-\frac{\Delta t}{R_1 C_1}} * V_{1,k} + R_1\left(1 - e^{-\frac{\Delta t}{R_1 C_1}}\right)\left(i_k - I_k^b\right), \tag{12}$$

$$V_{2,k+1} = e^{-\frac{\Delta t}{R_2 C_2}} * V_{2,k} + R_2\left(1 - e^{-\frac{\Delta t}{R_2 C_2}}\right)\left(i_k - I_k^b\right) \tag{13}$$

3.2 Hysteresis Effect and Parameter Identification

Plett (2004) illustrated the hysteresis effect by showing the lithium-ion polymer batteries' OCV-SOC charging and discharging curves at a C/25 current rate and ambient temperature. The difference between the two terminal voltages exists across the whole SOC range. Most part of the voltage difference is caused by the hysteresis effect, while only a small part of it is due to R_0 i_k drop. V. Srinivasan et al. (2001) gained insight into the hysteresis during the exchange of protons in nickel hydroxide by measuring and comparing the boundary curves from films of different structure (pure Ni, cobalt doped Ni, and aged films). Also, they evaluate various theories that have been proposed to explain the hysteresis effect. In order to model the slow transition by adding a "hysteresis state" to the battery model, Plett (2004) proposed a discrete-time equation (assuming $i(t)$ and $M(z, \dot{z})$ are constant over the sample period):

$$h_{k+1} = \exp\left(-\left|\frac{\eta_i i_k \gamma \Delta t}{C_n}\right|\right) h_k + \left(1 - \exp\left(-\left|\frac{\eta_i i_k \gamma \Delta t}{C_n}\right|\right)\right) M(z, \dot{z}) \tag{14}$$

Here η_i is the coulombic efficiency, γ is a positive constant, which tunes the rate of decay, C_n is the available capacity, and $M(z, \dot{z})$ is a function that gives the maximum polarization due to hysteresis as a function of SOC and the rate-of-change of SOC. Specifically, $M(z, \dot{z})$ is positive for charge ($\dot{z} > 0$) and is negative for discharge ($\dot{z} < 0$). From papers (Plett, 2004) and (Hu et al., 2012), we know the M is set to a fixed value, which is calculated by choosing the absolute maximum value from the voltage difference between charged OCV-SOC and discharged OCV-SOC curves as shown in **Figure 5**. In this case, the M = 0.0135V. To improve the model accuracy, one-state hysteresis is also considered in this paper.

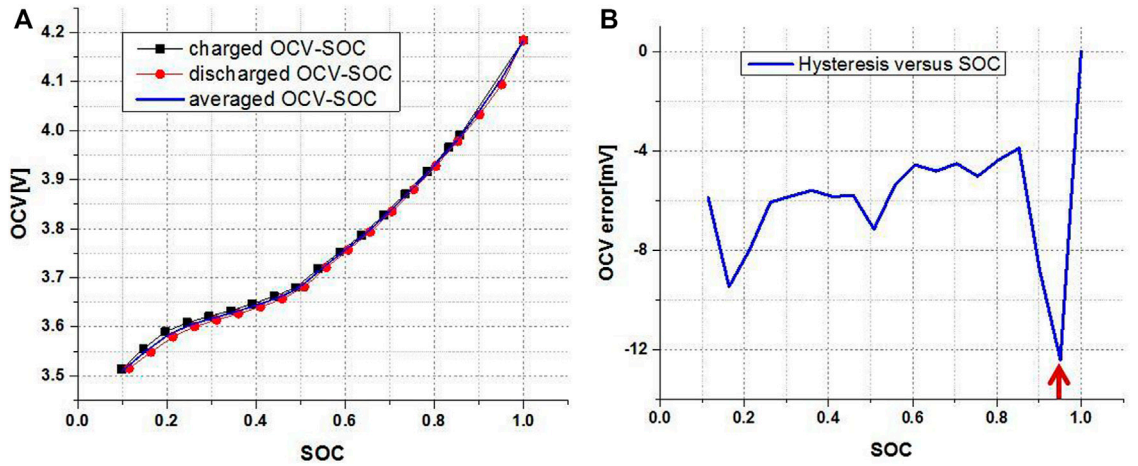

FIGURE 5 | (A) OCV-SOC curves; **(B)** OCV error (half of the difference of charged data minus discharged data).

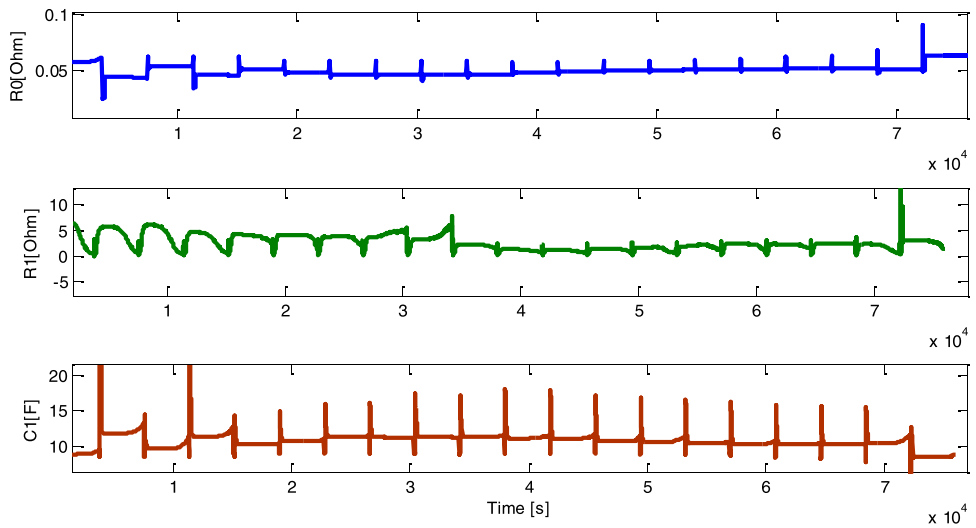

FIGURE 6 | 1RC-ECM parameters using RLS based on HPPC data.

To improve the estimated SOC accuracy, an actuated battery model is needed in model-based estimators (Chen et al., 2021). The key part to guaranteeing the model's accuracy is to identify the model parameters in an appropriate way. The recursive least squares (RLS) algorithm is one of the most widely used online parameters identification algorithms (Wang et al., 2017; Xiong et al., 2013b; Chen et al., 2015; Duong et al., 2015). Normally, the HPPC data is used to identify the model parameters. For example, the 1RC-ECM parameter are identified using the RLS as shown in **Figure 6**. If the model parameters are used to estimate the SOC based on EKF in each time step or by combining the RLS with the EKF to estimate the SOC (Arasaratnam et al., 2014), the EKF-based estimator will diverge easily due to the dramatically changed parameters. Dual EKF and joint EKF (Plett, 2005) may be an option for simultaneous SOC estimation, however, the complexity and relatively high computation requirements will drag it from a real application.

For the offline parameter identification method, the genetic algorithm (GA) is normally used to identify the model parameters by minimizing the error between the estimated terminal voltage, and the measured terminal voltage as shown in **Figure 7**. In this research, all the model parameters are identified using the GA method based on the ambient temperature HPPC data.

4 KEY FEATURES OF THE PROPOSED ESTIMATORS

In the literature, there are so many papers that describe the equations of the KF-based estimators, so in this part, only the key

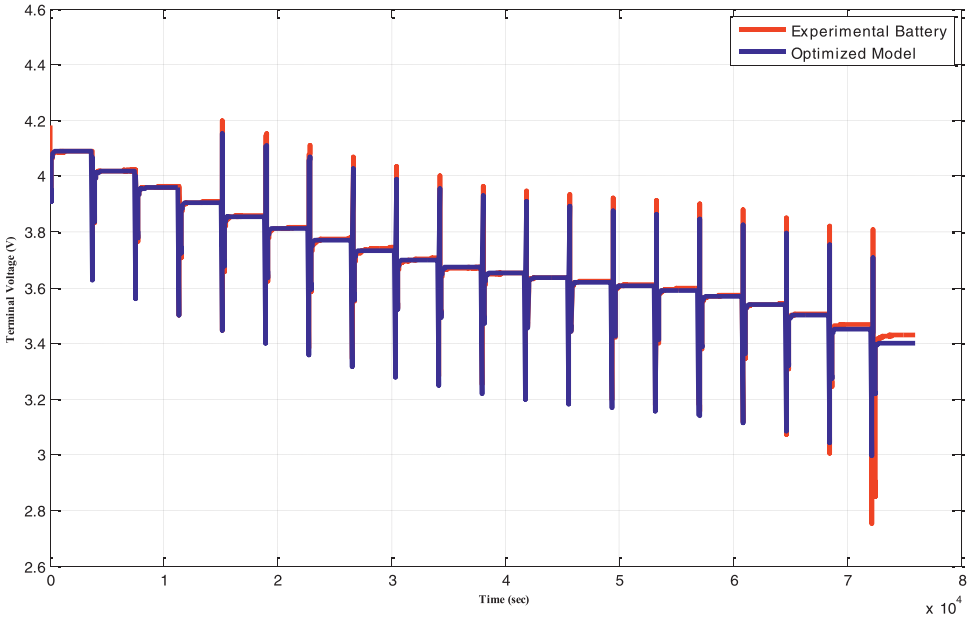

FIGURE 7 | 1RC-ECM optimized terminal voltage versus measured voltage using GA.

features in the process of implementing these algorithms are discussed here.

4.1 Two Versions of Adaptive Laws for Q and R Tuning

To ensure the KF-based estimator's convergence and to improve the estimated SOC accuracy, the process noise matrix Q and measurement noise matrix R need to be well tuned by the trial-and-error method, which is unlikely to be used in real EVs due to the complex operation conditions (Ruan et al., 2021). So, to improve the robustness of the estimators, two adaptive laws are then proposed to update the $\boldsymbol{Q}$ and $\boldsymbol{R}$ iteratively, one is an adaptive law with moving windows (Law 1) (Xiong et al., 2013c) and the other is an adaptive law with a forgetting factor (Law 2) (Hongwen He et al., 2011), the details are shown as follows:

a. Adaptive law with moving windows

$$H_k = \frac{1}{M}\sum_{i=k-M+1}^{k} e_k e_k^T$$
$$R_k = H_k - C_k P_{\overline{k}} C_k^T$$
$$Q_k = K_k H_k K_k^T$$

where H_k is the innovation covariance matrix based on the innovation sequence inside a moving estimation window of size M.

b. Adaptive law with a forgetting factor

The system model is described as follows:

$$\begin{cases} X_k = A_{k-1}X_{k-1} + B_{k-1}u_{k-1} + \Gamma_{k-1}w_{k-1} \\ Y_k = C_k X_k + D_k u_k + v_k \\ v_k \sim (r_k, R_k) \\ w_k \sim (q_k, Q_k) \end{cases}$$

where $d_k = \frac{1-\lambda}{1-\lambda^{k+1}}$, $0< \lambda <1$, where λ is called forgetting factor.

$$\hat{q}_{k+1} = (1-d_k)\hat{q}_k + d_k G_k\left[\hat{X}_{k+1} - A_k\hat{X}_k - B_k u_k\right]$$
$$\hat{Q}_{k+1} = (1-d_k)\hat{Q}_k + d_k G_k\left[K_{k+1}e_{k+1}e_{k+1}^T K_{k+1}^T + P_{k+1} - A_k P_k A_k^T\right]G_k^T$$
$$\hat{r}_{k+1} = (1-d_k)\hat{r}_k + d_k\left[Y_{k+1} - C_k\hat{X}_{k+1}^- - D_k u_k\right]$$
$$\hat{R}_{k+1} = (1-d_k)\hat{R}_k + d_k\left[e_{k+1}e_{k+1}^T - C_{k+1}P_{k+1}^- C_{k+1}^T\right]$$

where $G_k = [\Gamma_k^T\Gamma_k^-]^{-1}\Gamma_k^T$; error matrix $e_{k+1} = Y_{k+1} - C_{k+1}(A_{k+1}\hat{X}_{\overline{k+1}} + B_{k+1}u_{k+1}) - D_{k+1}u_{k+1} - \hat{r}_k$; gain matrix $K_{k+1} = P_{k+1}^- C_{k+1}^T[C_{k+1}P_{k+1}^- C_{k+1}^T + \hat{R}_k]^{-1}$; and estimate of the convariance $P_{k+1}^- = A_k P_k A_k^T + \Gamma_k\hat{Q}_k\Gamma_k^T$ and $P_{k+1} = (I - K_{k+1}C_{k+1})P_{k+1}^-$.

4.2 UKF With Two Types of Noise

For EKF, a Taylor-series expansion is used to linearize the nonlinear system by only considering the first-order term, this assumption will definitely lose some estimated accuracy when the system has much stronger nonlinearity. The UKF uses a statistical approach called the Unscented Transformation (UT) to handle the nonlinearity.

$$\lambda = \alpha^2(L+\kappa) - L$$
$$\eta_0^m = \lambda/(L+\lambda)$$

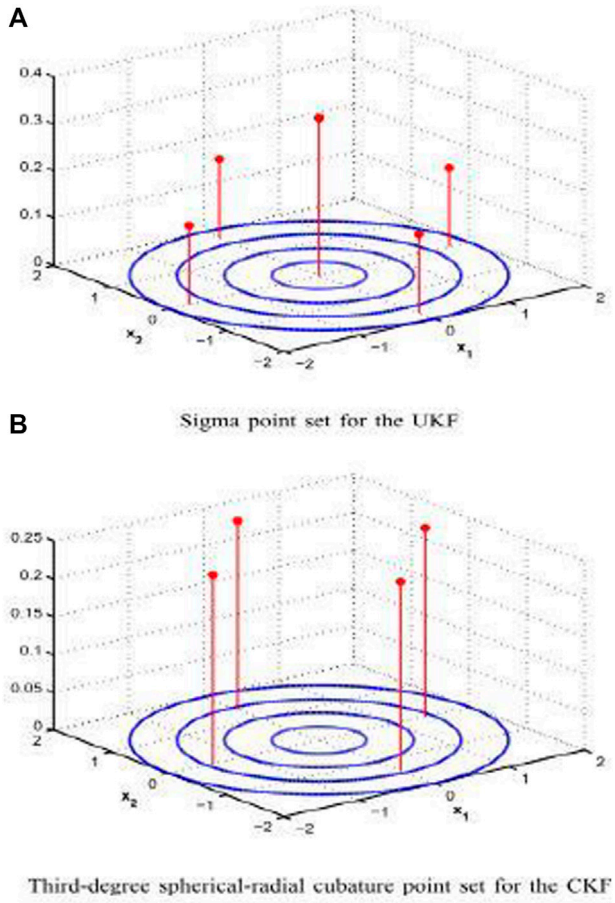

FIGURE 8 | Two kinds of distributions of point sets in two-dimensional space.

$$\eta_0^c = \lambda/(L+\lambda) + 1 - \alpha^2 + \beta$$
$$\eta_i^m = \eta_i^c = 1/[2(L+\lambda)],\ i = 1, \ldots, 2L$$
$$\chi_{k-1} = \left[\hat{x}_{k-1} \quad \hat{x}_{k-1} + \sqrt{L+\lambda}\sqrt{P_{k-1}} \quad \hat{x}_{k-1} - \sqrt{L+\lambda}\sqrt{P_{k-1}}\right]$$

where α, β, κ are the scaling parameters (default $= 1, \beta = 2, \kappa = 0$), L is the length of the state vector.

In general, there are two types of UKF (Rhudy and Gu, 2013), one is standard (un-augment) UKF and the other one is augmented UKF, the main difference is how to handle the noise. For standard UKF, the process and measurement noise terms are assumed to be additive, as in

$$x_k = f(x_{k-1}, u_{k-1}) + w_{k-1}$$
$$y_k = h(x_k, u_k) + v_k$$

The augmented UKF is

$$x_k = f(x_{k-1}, u_{k-1}, w_{k-1})$$
$$y_k = h(x_k, u_k, v_k)$$

To improve the SOC estimation accuracy and stability of the estimator, adaptive UKF (Sun et al., 2011) and square root unscented KF (SRUKF) (Zhou et al., 2015) are used to estimate the SOC. The implementation of UKF and the comparison study between EKF and UKF are shown in detail in the work of Rhudy and Gu (2013), and further study could be seen in the work ofRhudy et al. (2013).

4.3 Cubature Kalman Filter

CKF was first proposed by Arasaratnam and Haykin (2009), which shares the common characteristics with UKF, the main difference is how to generate the sigma points, as shown in **Figure 8**. For UKF, there are 2n+1 sigma point, while there are 2n sigma points for CKF. The other difference is that CKF needs to recalculate the covariance matrix and sigma points as shown in the following two equations (Wei et al., 2016):

$$S_{k|k-1} = chol\left(P_{k|k-1}\right)$$
$$\chi_{k|k-1}^{(i)} = S_{k|k-1}\xi^{(i)} + \hat{x}_{k|k-1},\ i = 1, 2, \ldots, 2n$$

4.4 H-Infinity Filter

Compared with the KF-based estimators, the H-infinity filter does not need the exact and known statistical properties of the system and measurement errors, and it still guarantees the estimation accuracy in the worst noise case. Although the theory of H-infinity is easy to understand, different forms of H-infinity and their complexity in coding have limited its application. Here, based on the work of Xue-min and Deng (1997), VanAntwerp and Braatz (2000), Zhang and Han (2008), and Lin et al. (2016), an easily understood and coding H-infinity filter is proposed as follows.

Recall that the system model is formulated as

$$x_k = Ax_{k-1} + Bu_k + w_k$$
$$y_k = Cx_k + Du_k + v_k$$
$$z_k = Lx_k$$

The $H\infty$ filter is required to provide a uniformly small estimation error $e_k = z_k - \hat{z}_k$ for any w_k, v_k. The measurement of performance is then given by

$$J = \frac{\sum_{k=0}^{N-1}\left\|Z_k - \hat{Z}_k\right\|_{\mathrm{Qk}}^2}{\left\|x_0 - \hat{x}_0\right\|_{\mathrm{po}^{-1}}^2 + \sum_{k=0}^{N-1}\left\{\|W_k\|^2 Wk^{-1} + \|v_k\|_{V_k}^2 - 1\right\}}$$

The performance criterion becomes

$$\min_{\hat{z}_k}\max_{(w_k, v_k, x_0)} J = -\frac{1}{2\gamma}\|x_0 - \hat{x}_0\|_{p_0^{-1}}^2 + \frac{1}{2}\sum_{k=0}^{N-1}\left\{\|z_k - \hat{z}_k\|_{Q_k}^2 - \frac{1}{\gamma}\left(\|w_k\|_{W_k^{-1}}^2 + \|v_k\|_{V_k^{-1}}^2\right)\right\}$$

In an SOC estimation problem, the noise w_k is mainly caused by current noise $w_k^{'}$, the weighting factor is $Q_k^{'}$, and then,

$$w_k = Bw_k^{'}$$
$$Q_k = BQ_k^{'}B^T$$
$$\bar{S}_k = L^T S_k L$$
$$T_k = \left(I - \theta\bar{S}_k P_k + C_k^T R^{-1} C_k P_k\right)$$

TABLE 2 | AEKF with forgetting factor $\lambda = 0.95$

RC branches	Mixed driving cycles		UDDS	
	MSE	Mean SOC error	MSE	Mean SOC error
1	1.98E-04	1.3239%	3.15E-04	1.7134%
1 + one hysteresis	**6.17E-05**	**0.4364%**	**1.04E-04**	**0.8492%**
2	1.24E-04	0.5516%	1.63E-04	0.9438%
2 + one hysteresis	5.88E-04	2.2836%	6.77E-05	0.4469%
3	2.93E-04	1.5535%	1.19E-04	0.9428%
3 + one hysteresis	1.38E-04	0.8781%	1.38E-04	1.0278%

The bold values in the mentioned tables are the minimum values.

TABLE 3 | Time consuming of AEKF with varying RC branches.

RC branches	Mixed driving cycles	UDDS
1	0.623414	0.874592
1 + one hysteresis	0.704906	0.993805
2	0.683496	0.979811
2 + one hysteresis	0.764954	1.09408
3	0.704004	1.013164
3 + one hysteresis	0.873314	1.272123

TABLE 4 | AUKF with moving windows M = 150.

RC branches	Mixed driving cycles		UDDS	
	MSE	Mean SOC error	MSE	Mean SOC error
1	**6.36E-05**	**0.4978%**	**4.82E-05**	**0.4792%**
1 + one hysteresis	5.90E-05	0.3832%	5.11E-05	0.2934%
2	2.65E-04	1.3504%	8.70E-05	0.4232%
2 + one hysteresis	3.13E-04	1.5724%	1.03E-04	0.7738%
3	9.80E-05	0.4865%	9.85E-05	0.716%
3 + one hysteresis	1.05E-04	0.7356%	5.80E-05	0.4036%

The bold values in the mentioned tables are the minimum values.

TABLE 5 | Time consuming of AUKF with varying RC branches.

RC branches	Mixed driving cycles	UDDS
1	**2.619153**	**3.810963**
1 + one hysteresis	3.290903	4.774251
2	3.231504	4.653444
2 + one hysteresis	3.93948	5.66124
3	3.829177	5.480512
3 + one hysteresis	4.682725	6.790386

The bold values in the mentioned tables are the minimum values.

TABLE 6 | ACKF with moving windows M = 150.

RC branches	Mixed driving cycles		UDDS	
	MSE	Mean SOC error	MSE	Mean SOC error
1	**7.44E-05**	**0.3895%**	**1.15E-04**	**0.8643%**
1 + one hysteresis	1.63E-04	0.9603%	8.09E-05	0.508%
2	4.13E-04	1.8038%	1.50E-04	1.0084%
2 + one hysteresis	6.48E-04	2.2831%	1.35E-04	0.9548%
3	6.53E-05	0.334%	1.17E-04	0.5374%
3 + one hysteresis	8.63E-05	0.5656%	1.02E-04	0.6082%

The bold values in the mentioned tables are the minimum values.

TABLE 7 | Time consuming of ACKF with varying RC branches.

RC branches	Mixed driving cycles	UDDS
1	2.306256	3.343073
1 + one hysteresis	2.848857	4.093163
2	2.793222	4.013798
2 + one hysteresis	3.391637	4.915385
3	3.35171	4.817241
3 + one hysteresis	4.020114	5.840877

TABLE 8 | H-infinity filter with varying RC branches.

RC branches	Mixed driving cycles		UDDS	
	MSE	Mean SOC error	MSE	Mean SOC error
1	4.86E-05	0.3954%	8.69E-05	0.5736%
1 + one hysteresis	2.94E-05	0.2708%	5.48E-05	0.5054%
2	2.91E-04	1.5093%	1.24E-04	0.7432%
2 + one hysteresis	4.29E-04	1.8134%	3.20E-04	1.633%
3	**5.75E-05**	**0.2649%**	**6.28E-05**	**0.4335%**
3 + one hysteresis	6.87E-05	0.3182%	7.84E-05	0.6082%

The bold values in the mentioned tables are the minimum values.

TABLE 9 | Time consumption of H-infinity with varying RC branches.

RC branches	Mixed driving cycles	UDDS
1	0.411761	0.571345
1 + one hysteresis	0.515896	0.716525
2	0.448291	0.633399
2 + one hysteresis	0.531628	0.750855
3	**0.46535**	**0.654545**
3 + one hysteresis	0.59286	0.847776

The bold values in the mentioned tables are the minimum values.

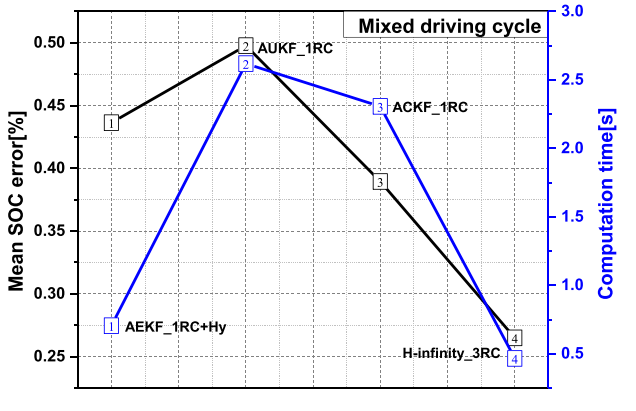

FIGURE 9 | Comparison results of the four estimators with white noise.

$$K_k = AP_kT_kC_k^TR^{-1}$$

$$\hat{x}_{k+1} = A\hat{x}_k + Bu_k + K_k\left[y_k - \left(OCV\left(\widehat{soc}_k\right) + R_0u_k + \hat{x}_{k,2} + \hat{x}_{k,3}\right)\right]$$

$$P_{k+1} = AP_kT_kA^T + BQ_k^{'}B^T$$

5 SIMULATION RESULTS AND DISCUSSION

In this part, the normal ECM and augmented ECM with varying RC branches and hysteresis effects are combined with the four proposed estimators (EKF, UKF, CKF, and H-infinity) to estimate the SOC under different noise assumptions. And the model parameters are identified by GA using ambient temperature HPPC data. The temperature and aging effects are not considered here. For the noise assumptions, the voltage noise is fixed type, which is 5mV (the mainstream voltage sensors' accuracy level) + 0.5 V amplitude white noise. While for the current noise assumptions, firstly, only the 0.5 A amplitude white noise are added to the current data, the estimation results are discussed in **Section 5.1**. Secondly, the 1% of 1C-rate bias current noise (0.022 A)+ 0.5 A amplitude white noise is used to contaminate the tested current data. The estimated SOC results are discussed in **Section 5.2**. Lastly, to evaluate the robustness of the proposed estimators, the 5%, 10%,

TABLE 10 | AEKF with 1% current bias noise added.

RC branches	Mixed driving cycles		UDDS	
	MSE	Mean SOC error	MSE	Mean SOC error
1	**2.96E-04**	**1.348%**	**3.45E-04**	**1.5174%**
1 + one hysteresis	2.57E-04	1.1654%	6.57E-04	2.15%
2	3.79E-04	1.634%	0.001234	2.8858%
2 + one hysteresis	0.002619	4.6574%	0.00148	3.3015%
3	4.56E-04	1.7456%	5.35E-04	1.5442%
3 + one hysteresis	6.92E-04	2.1506%	3.61E-04	1.4472%

The bold values in the mentioned tables are the minimum values.

TABLE 11 | AUKF with 1% current bias noise added.

RC branches	Mixed driving cycles		UDDS	
	MSE	Mean SOC error	MSE	Mean SOC error
1	**2.70E-04**	**1.4355%**	**4.69E-04**	**1.7026%**
1 + one hysteresis	4.44E-04	1.8238%	3.85E-04	1.6367%
2	0.001196	3.0985%	8.65E-04	2.5085%
2 + one hysteresis	0.001379	3.3542%	0.00106	2.8208%
3	3.42E-04	1.5551%	2.24E-04	1.1264%
3 + one hysteresis	4.03E-04	1.736%	3.92E-04	1.6129%

The bold values in the mentioned tables are the minimum values.

TABLE 12 | ACKF with 1% current bias noise added.

RC branches	Mixed driving cycles		UDDS	
	MSE	Mean SOC error	MSE	Mean SOC error
1	**1.51E-04**	**0.9793%**	**3.55E-04**	**1.4404%**
1 + one hysteresis	7.02E-04	2.2454%	0.001288	2.9048%
2	9.60E-04	2.7682%	7.25E-04	2.3733%
2 + one hysteresis	0.001321	3.3247%	0.001235	3.1532%
3	2.87E-04	1.4025%	7.09E-04	2.1438%
3 + one hysteresis	8.70E-04	2.5454%	7.80E-04	2.4736%

The bold values in the mentioned tables are the minimum values.

TABLE 13 | H-infinity filter with 1% current bias noise added.

RC branches	Mixed driving cycles		UDDS	
	MSE	Mean SOC error	MSE	Mean SOC error
1	**2.04E-04**	**1.1447%**	**1.83E-04**	**1.156%**
1 + one hysteresis	7.80E-04	2.329%	8.46E-04	1.6538%
2	9.76E-04	2.7704%	6.43E-04	2.2911%
2 + one hysteresis	0.00149	3.4699%	0.001226	3.1828%
3	2.13E-04	1.2097%	5.08E-04	1.8536%
3 + one hysteresis	8.59E-04	2.4864%	0.001154	2.9956%

The bold values in the mentioned tables are the minimum values.

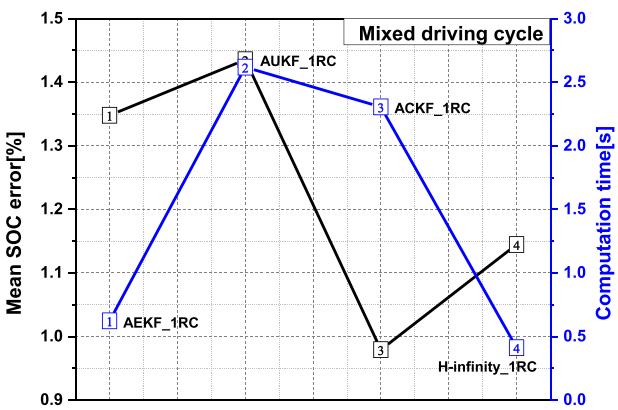

FIGURE 10 | Comparison results of the four estimators with 1% current bias.

20%, and random bias (with 0.44 A amplitude) of 1C-rate bias noise+ 0.5 A amplitude white noise are added into the tested current data, the estimation results are discussed in **Section 5.3**.

5.1 Estimation Results With Only White Noise

In this study, the two aforementioned adaptive laws are the moving window version and the forgetting factor version. It is worth mentioning that the forgetting factor adaptive law seems to be more suitable for the EKF since the moving window one needs to be well tuned due to its sensitivity to the preset initial SOC value. Here, since the adaptive laws are used to update the $\boldsymbol{Q}$, $\boldsymbol{R}$ iteratively in KF-based estimators, the initialized values of the $\boldsymbol{Q}$ and $\boldsymbol{R}$ related matrix could be set arbitrarily. In the following, I just show the initialized parameters which are used in the normal KF-based estimators; forgetting factor $\lambda = 0.95$, moving windows M = 150 for UKF and CKF, $\boldsymbol{p} = 0.01*eye(sN)$, $\boldsymbol{Q} = 0.01*eye(sN)$, $\boldsymbol{R}$

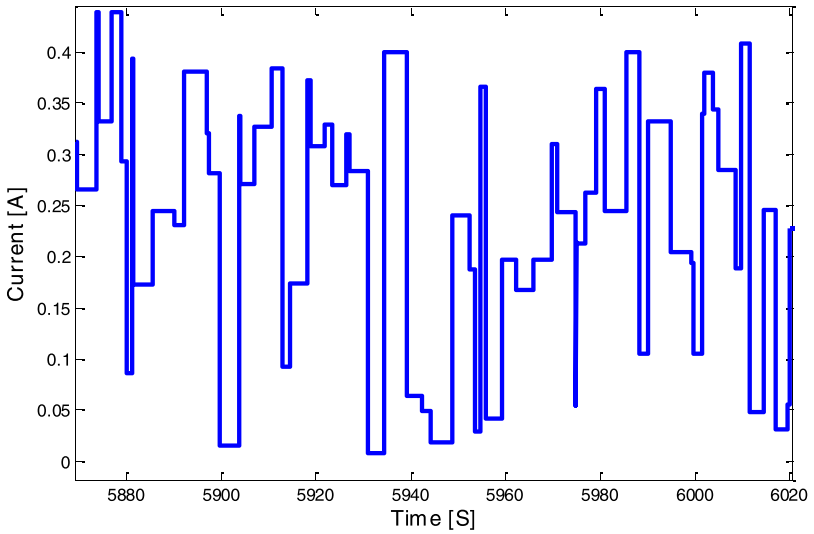

FIGURE 11 | Zoom-in of the random bias noise.

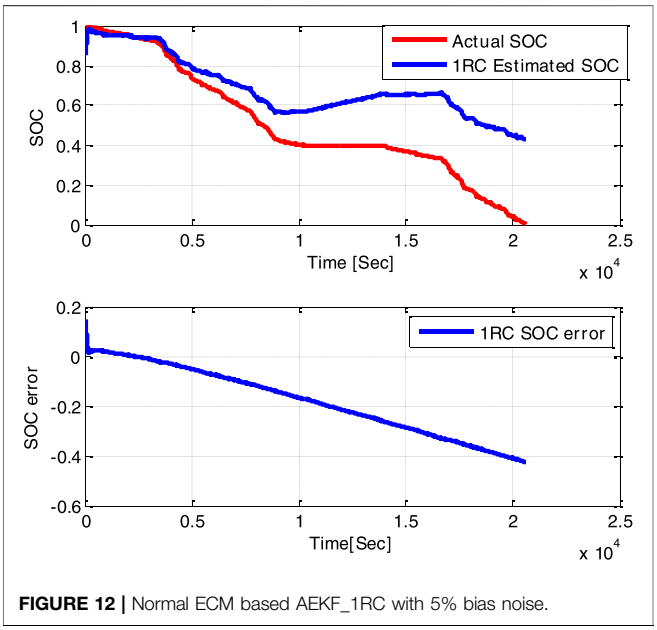

FIGURE 12 | Normal ECM based AEKF_1RC with 5% bias noise.

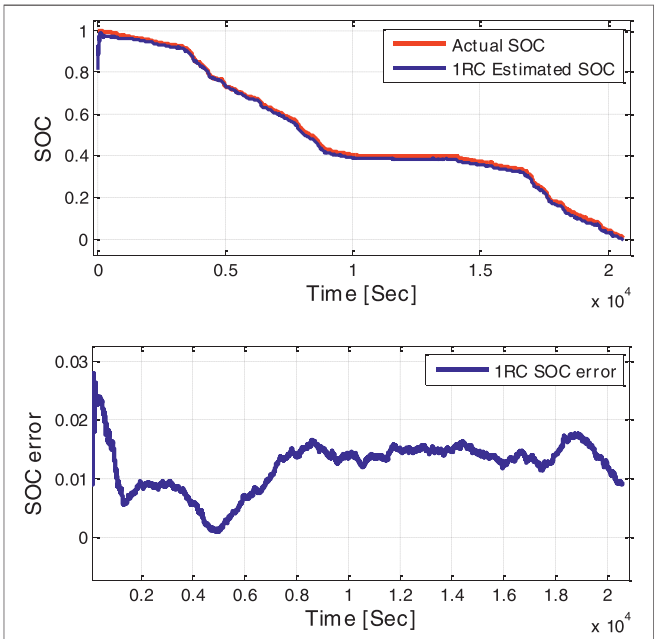

FIGURE 13 | Augmented ECM based AEKF_1RC with 5% bias noise.

= *0.01*, *sN* means state number, Γ, ***q***, ***r*** are also set to be 0.01 multiplying the number of rows and columns.

As shown in **Table 2**, the two driving cycles are used to evaluate the estimators, and it is obvious that the accuracy level for two types of data is not the same, which is caused by the fixed model parameters since the identified parameters may be more accurate and suitable for mixed driving cycles. For example, for mixed driving cycles, the 1RC + one hysteresis state has the best accuracy of 0.4364% mean SOC error, while in the UDDS case, the 2RC + one hysteresis state has the best accuracy of 0.4469%. It is well known that increasing RC branches will improve the model accuracy, however, if the model is accurate enough, more RC branches will cause the model overfitting problems as shown in the 2RC and 3RC cases. That is also the reason why in the following tables only up to 5RC branches ECM are studied since the aim of this research is to obtain the optimal estimator with relatively high accuracy level and less computation time-consuming. The more RC branches may decrease the model accuracy and increase the computation time, as shown in **Table 3**.

Similarly, **Tables 4–9** shows the simulation results of the UKF, CKF, and H-infinity filters only under the white noise assumption. The moving windows adaptive law is used for

TABLE 14 | Augmented ECM-based AEKF with 5% bias.

RC branches	Mixed driving cycles		UDDS	
	MSE	Mean SOC error	MSE	Mean SOC error
1	1.36E-04	0.9632%	1.64E-04	1.1243%
2	4.50E-04	1.7093%	2.01E-04	0.6632%
3	1.81E-04	0.931%	2.23E-04	1.1973%
4	**1.19E-04**	**0.521%**	**1.48E-04**	**0.9135%**
5	4.90E-04	1.8785%	1.14E-04	0.6326%

The bold values in the mentioned tables are the minimum values.

TABLE 15 | Augmented ECM-based AEKF with 10% bias.

RC branches	Mixed driving cycles		UDDS	
	MSE	Mean SOC error	MSE	Mean SOC error
1	2.11E-04	1.1581%	2.75E-04	1.5063%
2	4.76E-04	1.7761%	1.77E-04	0.8099%
3	2.17E-04	0.978%	2.19E-04	1.1829%
4	**2.42E-04**	**0.9167%**	**1.59E-04**	**0.7971%**
5	5.46E-04	1.9776%	1.40E-04	0.6529%

The bold values in the mentioned tables are the minimum values.

TABLE 16 | Augmented ECM-based AEKF with 20% bias.

RC branches	Mixed driving cycles		UDDS	
	MSE	Mean SOC error	MSE	Mean SOC error
1	3.41E-04	1.5457%	2.41E-04	1.3191%
2	0.001056	1.9063%	3.98E-04	0.8321%
3	2.77E-04	1.1942%	3.06E-04	1.4411%
4	**3.02E-04**	**0.7748%**	**2.43E-04**	**1.0609%**
5	7.52E-04	1.886%	2.56E-04	0.6159%

The bold values in the mentioned tables are the minimum values.

TABLE 17 | Augmented ECM-based AEKF with 20% random bias.

RC branches	Mixed driving cycles		UDDS	
	MSE	Mean SOC error	MSE	Mean SOC error
1	2.43E-04	1.3523%	2.75E-04	1.5172%
2	3.96E-04	1.5051%	1.98E-04	0.5954%
3	2.84E-04	1.3446%	2.62E-04	1.3528%
4	**1.35E-04**	**0.5697%**	**1.59E-04**	**0.9525%**
5	3.55E-04	1.5232%	8.91E-05	0.4184%

The bold values in the mentioned tables are the minimum values.

UKF and CKF, the reason is that the Cholesky factorization of covariance matrix $\boldsymbol{P}$ in the algorithms is more sensitive to the forgetting factor, which means the inappropriate λ may cause the $\boldsymbol{P}$ to violate the positive definite requirement for the Chol($\boldsymbol{P}$). From the simulation results, it is obvious that the UKF and CKF is more accurate than the EKF compared with the same order RC model, which is reasonable since the UKF and CKF use the sigma points to deal with the nonlinearity of the model while the EKF only uses the first order Taylor series linearization process. The strategy used in the UKF and CKF is much more accurate than

TABLE 18 | Time consumption of the augmented ECM-based AEKF.

RC branches	Mixed driving cycles	UDDS
1	0.660001	0.942093
2	0.676165	0.949211
3	0.721047	1.015646
4	**0.735255**	**1.040624**
5	0.771258	1.078617

The bold values in the mentioned tables are the minimum values.

the EKF in dealing with the nonlinearity, however, the drawback of these two estimators is that they are too much more time consuming than the EKF, as shown in **Tables 5**, **7**.

So far, no adaptive law for the H-infinity filter, since it may still have good performance even in the worst noise case. The following shows the preset parameters for H-infinity estimation, $= 10^{-7}$, $Q_{\overline{k}}^{'} = 0.022$, $R = 0.005$, $L = (1\ 0\ 0)$ for 2RC, $S_k = 1$. The most attractive feature of the H-infinity filter is that it is the least time-consuming as shown in **Table 9**. All the four candidates with relatively high accuracy and less time-consuming in the proposed

TABLE 19 | Augmented ECM-based H-infinity with 5% bias.

RC branches	Mixed driving cycles		UDDS	
	MSE	Mean SOC error	MSE	Mean SOC error
1	**1.59E-04**	**1.0098%**	**7.79E-05**	**0.6183%**
2	0.001033	2.9521%	4.74E-04	1.8654%
3	2.08E-04	1.0933%	8.64E-05	0.5339%
4	3.86E-04	1.7233%	2.44E-04	1.2372%
5	0.00103	2.9569%	5.63E-04	1.938%

The bold values in the mentioned tables are the minimum values.

TABLE 20 | Augmented ECM-based H-infinity with 10% bias.

RC branches	Mixed driving cycles		UDDS	
	MSE	Mean SOC error	MSE	Mean SOC error
1	**1.64E-04**	**0.9558%**	**8.10E-05**	**0.5372%**
2	0.001043	2.9774%	5.60E-04	1.9919%
3	2.31E-04	1.0941%	1.23E-04	0.709%
4	5.58E-04	2.0764%	2.17E-04	1.1479%

The bold values in the mentioned tables are the minimum values.

TABLE 21 | Augmented ECM-based H-infinity with 20% bias.

RC branches	Mixed driving cycles		UDDS	
	MSE	Mean SOC error	MSE	Mean SOC error
1	**2.32E-04**	**1.0392%**	**1.28E-04**	**0.6748%**
2	0.001487	3.304%	7.92E-04	2.1894%
3	2.13E-04	1.0053%	1.87E-04	0.746%
4	5.23E-04	1.8832%	2.56E-04	1.1456%

The bold values in the mentioned tables are the minimum values.

TABLE 22 | Augmented ECM-based H-infinity with 20% random bias.

RC branches	Mixed driving cycles		UDDS	
	MSE	Mean SOC error	MSE	Mean SOC error
1	**7.62E-05**	**0.5281%**	**7.18E-05**	**0.4966%**
2	8.41E-04	2.6739%	3.91E-04	1.6731%
3	1.45E-04	0.8467%	1.01E-04	0.5642%
4	3.12E-04	1.5168%	2.01E-04	1.0527%

The bold values in the mentioned tables are the minimum values.

TABLE 23 | Time consumption of the augmented ECM-based H-infinity.

RC branches	Mixed driving cycles	UDDS
1	**0.463775**	**0.652417**
2	0.495241	0.695954
3	0.53066	0.75639
4	0.573406	0.796384
5	0.614732	0.87387

The bold values in the mentioned tables are the minimum values.

estimators are shown in **Figure 9**, in which the H-infinity with 3RC is the optimal estimator under only white noise added assumption. Here, the KF is well known to be the optimal estimator under white noise assumption; however, in this case, the current data are assumed to be white noise added while the noise in the battery model may not be of Gaussian distribution, which leads to the H-infinity filter being the best option.

5.2 Estimation Results With 1% (1C-Rate) Current Bias Noise

The aforementioned results are only based on white noise assumptions, which is unlikely to happen in real EVs since the current sensors do have some bias noise disturbance. Here, 1% of 1C-rate bias noise + white noise is used to simulate the inaccurate current sensors in a real application. Since the battery model is not changed and the measurement noise (terminal voltage) is fixed in all estimation processes, the pre-set parameters for all the estimators remain the same as shown in **Section 5.1**. The estimation results are shown in **Tables 10**-**13**, it is obvious that all the estimated mean SOC errors with varying RC branches are slightly larger than the ones shown before, which means the current bias noise does have an effect on the SOC accuracy. The possible solution is to add one more state to the ECM to capture the noise variations as discussed in **Section 3.1**, and the effectiveness of the augmented ECM will be discussed later. In this part, since the data points of the current and voltage used here are the same as in **Section 5.1**, the computation time of the four estimators is not shown here. As shown in **Figure 10**, the ACKF_1RC has the least mean SOC error (0.9793%), however, the about 2.3 s computation time hinders it from being the optimal estimator, the H-infinity_1RC may be the best option with the tradeoff of accuracy and time-consuming.

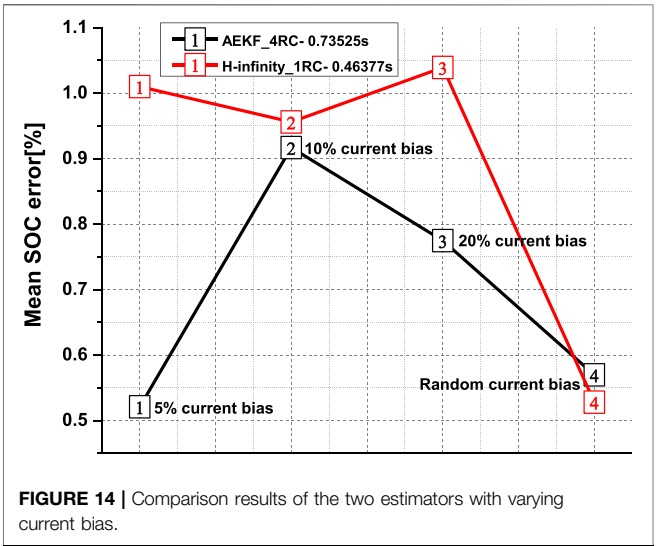

FIGURE 14 | Comparison results of the two estimators with varying current bias.

5.3 Estimation Results With 5–20% Bias Noise and Random Bias Noise

To validate the robustness of the augmented ECM based estimators, the 5, 10, 20% fixed bias and the 20% random bias current noise are added to the current data. The 20% random bias noise means the amplitude of the noise is 20% of the 1C-rate while the specific bias value is randomly generated, which could be partially seen in **Figure 11**. Compared with the SOC error using 1% current bias, when the 5% bias current noise is added to the current data, the absolute maximum SOC error of the normal ECM based AEKF estimator reaches about 40%, as shown in **Figure 12**, and a similar SOC error happens in the other three estimators. However, if the augmented ECM is used, the SOC error will decrease to about 1.5%, as shown in **Figure 13**. It is worth mentioning that the augmented ECM based UKF and CKF estimators could not decrease the SOC error, and the details of the reason are not discussed here. So, only the augmented ECM based EKF and H-infinity filter are compared with different current bias noise, and the estimated SOC error and the computation time are listed in **Tables 14**–**23**.

The estimated SOC error of the augmented ECM using the same RC branches increases with the varying bias noise. For example, the SOC error trend of the augmented ECM_1RC based AEKF is 0.9632% → 1.1581% →1.5457%, while the computation time of the normal ECM_1RC based AEKF and the augmented one is 0.623414 and 0.660001s, respectively. For the augmented ECM, the added state for noise estimation has a slight effect on the computation time, which means two or three more states could be added to the ECM to improve the robustness of the estimator when the accuracy of the current sensors is dramatically changed under complex driving conditions. The comparison results of the two estimators with varying bias noise are shown in **Figure 14**. The AEKF_4RC seems to have slightly better accuracy than the H-infinity_1RC, the possible reason may be that non-adaptive laws are used in the H-infinity based estimators, which means the ***Q, R*** related matrix are not tuned to their optimized values. However, H-infinity based estimators are still a potential candidate to be used in real applications considering their less time-consuming computation. In fact, the results of the robustness evaluation process show that the proposed two estimators are both suitable for SOC estimation.

6 CONCLUSION

In this paper, the three most proposed KF-based estimators (EKF, UKF, and CKF) and H-infinity filter in the SOC estimation research area are compared and evaluated based on the SOC accuracy and algorithms' complexity. Also, some basics of the SOC estimation are validated, such as constant current (0.5C-rate) with proper relaxation time (1 h) and SOC interval (5%) is more accurate than the small C-rate (0.02C-rate) charge/discharge to obtain the OCV-SOC curves, while the forgetting factor adaptive law is better for the EKF and the moving windows adaptive law is better in UKF and CKF. For the results of SOC estimation, the H-infinity filter is the optimal estimator to estimate the SOC with relatively higher accuracy and less computation time under Gaussian noise and 1% current bias noise, while for the worse bias noise assumption, the Augmented AEKF_4RC and H-infinity filter_1RC are both suitable for SOC estimation. Further work will be conducted in the state of power (SOP) and SOC joint estimation areas and the temperature and aging effects will also be considered.

DATA AVAILABILITY STATEMENT

The raw data supporting the conclusions of this article will be made available by the authors without undue reservation.

AUTHOR CONTRIBUTIONS

All authors listed have made a substantial, direct, and intellectual contribution to the work and approved it for publication.

REFERENCES

Ahmed, R., El Sayed, M., Arasaratnam, I., Tjong, J., and Habibi, S. (2014). Reduced-Order Electrochemical Model Parameters Identification and State of Charge Estimation for Healthy and Aged Li-Ion Batteries-Part II: Aged Battery Model and State of Charge Estimation. *IEEE J. Emerg. Sel. Top. Power Electron.* 2, 678–690. doi:10.1109/jestpe.2014.2331062

Arasaratnam, I., Tjong, J., and Ahmed, R. (2014). "Battery Management System in the Bayesian Paradigm: Part I: SOC Estimation," in 2014 IEEE Transportation Electrification Conference and Expo (ITEC), Dearborn, MI, USA, 15-18 June 2014 (IEEE), 1–5. doi:10.1109/itec.2014.6861863

Arasaratnam, I., and Haykin, S. (2009). Cubature Kalman Filters. *IEEE Trans. Autom. Contr.* 54, 1254–1269. doi:10.1109/tac.2009.2019800

Chen, C., Wei, Z., and Knoll, A. C. (2021). "Charging Optimization for Li-Ion Battery in Electric Vehicles: A Review," in IEEE Transactions on Transportation Electrification (IEEE). doi:10.1109/TTE.2021.3135525

Chen, Z., Xia, B., and Mi, C. C. (2015). "A Novel State-Of-Charge Estimation Method for Lithium-Ion Battery Pack of Electric Vehicles," in 2014 IEEE Transportation Electrification Conference and Expo (ITEC), Dearborn, MI, USA, 14-17 June 2015 (IEEE), 1–6. doi:10.1109/itec.2015.7165778

Cuma, M. U., and Koroglu, T. (2015). A Comprehensive Review on Estimation Strategies Used in Hybrid and Battery Electric Vehicles. *Renew. Sustain. Energy Rev.* 42, 517–531. doi:10.1016/j.rser.2014.10.047

Duong, V.-H., Bastawrous, H. A., Lim, K., See, K. W., Zhang, P., and Dou, S. X. (2015). Online State of Charge and Model Parameters Estimation of the LiFePO4 Battery in Electric Vehicles Using Multiple Adaptive Forgetting Factors Recursive Least-Squares. *J. Power Sources* 296, 215–224. doi:10.1016/j.jpowsour.2015.07.041

Hongwen He, H., Rui Xiong, R., Xiaowei Zhang, X., Fengchun Sun, F., and JinXin Fan, J. (2011). State-of-charge Estimation of the Lithium-Ion Battery Using an Adaptive Extended Kalman Filter Based on an Improved Thevenin Model. *IEEE Trans. Veh. Technol.* 60, 1461–1469. doi:10.1109/tvt.2011.2132812

Hu, J., Bian, X., Wei, Z., Li, J., and He, H. (2021). "Residual Statistics-Based Current Sensor Fault Diagnosis for Smart Battery Management," in IEEE Journal of Emerging and Selected Topics in Power Electronics (IEEE). doi:10.1109/JESTPE.2021.3131696

Hu, J., He, H., Wei, Z., and Li, Y. (2021). "Disturbance-immune and Aging-Robust Internal Short Circuit Diagnostic for Lithium-Ion Battery," in IEEE Transactions on Industrial Electronics (IEEE), 1988–1999. doi:10.1109/TIE.2021.3063968

Hu, J., Wei, Z., and He, H. (2021). An Online Adaptive Internal Short Circuit Detection Method of Lithium-Ion Battery. *Automot. Innov.* 4, 93–102. doi:10.1007/s42154-020-00127-9

Hu, X., Li, S., and Peng, H. (2012). A Comparative Study of Equivalent Circuit Models for Li-Ion Batteries. *J. Power Sources* 198, 359–367. doi:10.1016/j.jpowsour.2011.10.013

Kim, T., Wang, Y., Sahinoglu, Z., Wada, T., Hara, S., and Qiao, W. (2014). "State of Charge Estimation Based on a Realtime Battery Model and Iterative Smooth Variable Structure Filter," in IEEE Innovative Smart Grid Technologies-Asia (ISGT ASIA), Kuala Lumpur, Malaysia, 20-23 May 2014 (IEEE), 132–137. doi:10.1109/ISGT-Asia.2014.6873777

Li, Y., Wei, Z., Xiong, B., and Vilathgamuwa, D. M. (2021). "Adaptive Ensemble-Based Electrochemical-Thermal-Degradation State Estimation of Lithium-Ion Batteries," in IEEE Transactions on Industrial Electronics (IEEE). doi:10.1109/TIE.2021.3095815

Lin, C., Mu, H., Xiong, R., and Shen, W. (2016). A Novel Multi-Model Probability Battery State of Charge Estimation Approach for Electric Vehicles Using H-Infinity Algorithm. *Appl. Energy* 166, 76–83. doi:10.1016/j.apenergy.2016.01.010

Liu, K., Gao, Y., Li, K., Zhu, C., Fei, M., Peng, C., et al. (2022). Electrochemical Modeling and Parameterization towards Control-Oriented Management of Lithium-Ion Batteries. *Control Eng. Pract.* 124, 105176. doi:10.1016/j.conengprac.2022.105176

Liu, K., Wei, Z., Zhang, C., Shang, Y., Teodorescu, R., and Han, Q-L. (2022). "Towards Long Lifetime Battery: AI-Based Manufacturing and Management," in IEEE/CAA Journal of Automatica Sinica (IEEE). doi:10.1109/jas.2022.105599

Lu, L., Han, X., Li, J., Hua, J., and Ouyang, M. (2013). A Review on the Key Issues for Lithium-Ion Battery Management in Electric Vehicles. *J. power sources* 226, 272–288. doi:10.1016/j.jpowsour.2012.10.060

Plett, G. L. (2005). "Dual and Joint EKF for Simultaneous SOC and SOH Estimation," in Proceedings of the 21st Electric Vehicle Symposium (EVS21), Monaco, 2005, April 2-6 (Monaco), 1–12.

Plett, G. L. (2004). Extended Kalman Filtering for Battery Management Systems of LiPB-Based HEV Battery Packs. *J. Power Sources* 134, 262–276. doi:10.1016/j.jpowsour.2004.02.032

Rhudy, M., and Gu, Y. (2013). Understanding Nonlinear Kalman Filters, Part Ii: an Implementation Guide. *Interact. Robot. Lett.* 1, 18. doi:10.2514/6.2013-5198

Rhudy, M. B., Gu, Y., and Napolitano, M. (2013). "Does the Unscented Kalman Filter Converge Faster Than the Extended Kalman Filter? A Counter Example," in AIAA Guidance, Navigation, and Control (GNC) Conference2013. Boston, MA, USA, 2013. August 19-22 (GNC), 5198.

Ruan, H., He, H., Wei, Z., Quan, Z., and Li, Y. (2021). "State of Health Estimation of Lithium-Ion Battery Based on Constant-Voltage Charging Reconstruction," in IEEE Journal of Emerging and Selected Topics in Power Electronics (IEEE). doi:10.1109/jestpe.2021.3098836

Srinivasan, V., Weidner, J. W., and Newman, J. (2001). Hysteresis during Cycling of Nickel Hydroxide Active Material. *J. Electrochem. Soc.* 148, A969. doi:10.1149/1.1385846

Sun, F., Hu, X., Zou, Y., and Li, S. (2011). Adaptive Unscented Kalman Filtering for State of Charge Estimation of a Lithium-Ion Battery for Electric Vehicles. *Energy* 36, 3531–3540. doi:10.1016/j.energy.2011.03.059

U.S. Department of Energy (2001). *PNGV Battery Test Manual*. DOE/ID-10597. Idaho Falls: Lockheed Idaho Technologies Co.

VanAntwerp, J. G., and Braatz, R. D. (2000). A Tutorial on Linear and Bilinear Matrix Inequalities. *J. process control* 10, 363–385. doi:10.1016/s0959-1524(99)00056-6

Wang, Y., Tian, J., Sun, Z., Wang, L., Xu, R., Li, M., et al. (2020). A Comprehensive Review of Battery Modeling and State Estimation Approaches for Advanced Battery Management Systems. *Renew. Sustain. Energy Rev.* 131, 110015. doi:10.1016/j.rser.2020.110015

Wang, Y., Zhang, C., and Chen, Z. (2017). On-line Battery State-Of-Charge Estimation Based on an Integrated Estimator. *Appl. Energy* 185, 2026–2032. doi:10.1016/j.apenergy.2015.09.015

Wei, Z., He, H., Pou, J., Tsui, K-L., Quan, Z., and Li, Y. (2020). "Signal-disturbance Interfacing Elimination for Unbiased Model Parameter Identification of Lithium-Ion Battery," in IEEE Transactions on Industrial Informatics (IEEE), 5887–5897. doi:10.1109/TII.2020.3047687

Wei, Z., Hu, J., He, H., Yu, Y., and Marco, J. (2022). "Embedded Distributed Temperature Sensing Enabled Multi-State Joint Observation of Smart Lithium-Ion Battery," in IEEE Transactions on Industrial Electronics (IEEE). doi:10.1109/tie.2022.3146503

Wei, Z., Quan, Z., Wu, J., Li, Y., Pou, J., and Zhong, H. (2021). "Deep Deterministic Policy Gradient-Drl Enabled Multiphysics-Constrained Fast Charging of Lithium-Ion Battery," in IEEE Transactions on Industrial Electronics (IEEE), 2588–2598. doi:10.1109/TIE.2021.3070514

Wei, Z., Ruan, H., Li, Y., Li, J., Zhang, C., and He, H. (2022). "Multi-Stage State of Health Estimation of Lithium-Ion Battery with High Tolerance to Heavily-Partial Charging," in IEEE Transactions on Power Electronics (IEEE). doi:10.1109/tpel.2022.3144504

Wei, Z., Zhao, J., Xiong, R., Dong, G., Pou, J., and Tseng, K. J. (2018). "Online Estimation of Power Capacity with Noise Effect Attenuation for Lithium-Ion Battery," in IEEE Transactions on Industrial Electronics (IEEE), 5724–5735. doi:10.1109/TIE.2018.2878122

Wei, Z., Zou, C., Leng, F., Soong, B. H., and Tseng, K-J. (2017). "Online Model Identification and State-Of-Charge Estimate for Lithium-Ion Battery with a Recursive Total Least Squares-Based Observer," in IEEE Transactions on Industrial Electronics (IEEE), 1336–1346. doi:10.1109/TIE.2017.2736480

Wei, Z. G., Hu, J., He, H., Li, Y., and Xiong, B. (2021). "Load Current and State of Charge Co-estimation for Current Sensor-free Lithium-Ion Battery," in IEEE Transactions on Power Electronics (IEEE). doi:10.1109/tpel.2021.3068725

Wei, Z., Hu, J., Li, Y., He, H., Li, W., and Sauer, D. U. (2022). Hierarchical Soft Measurement of Load Current and State of Charge for Future Smart Lithium-Ion Batteries. *Appl. Energy* 307, 118246. doi:10.1016/j.apenergy.2021.118246

Wei, Z., Meng, S., Xiong, B., Ji, D., and Tseng, K. J. (2016). Enhanced Online Model Identification and State of Charge Estimation for Lithium-Ion Battery with a FBCRLS Based Observer. *Appl. energy* 181, 332–341. doi:10.1016/j.apenergy.2016.08.103

Wei, Z., Zhao, D., He, H., Cao, W., and Dong, G. (2020). A Noise-Tolerant Model Parameterization Method for Lithium-Ion Battery Management System. *Appl. Energy* 268, 114932. doi:10.1016/j.apenergy.2020.114932

Wei, Z., Zhao, J., He, H., Ding, G., Cui, H., and Liu, L. (2021). Future Smart Battery and Management: Advanced Sensing from External to Embedded Multi-Dimensional Measurement. *J. Power Sources* 489, 229462. doi:10.1016/j.jpowsour.2021.229462

Xia, B., Wang, H., Tian, Y., Wang, M., Sun, W., and Xu, Z. (2015). State of Charge Estimation of Lithium-Ion Batteries Using an Adaptive Cubature Kalman Filter. *Energies* 8, 5916–5936. doi:10.3390/en8065916

Xiong, R., Gong, X., Mi, C. C., and Sun, F. (2013). A Robust State-Of-Charge Estimator for Multiple Types of Lithium-Ion Batteries Using Adaptive Extended Kalman Filter. *J. Power Sources* 243, 805–816. doi:10.1016/j.jpowsour.2013.06.076

Xiong, R., Sun, F., Gong, X., and He, H. (2013). Adaptive State of Charge Estimator for Lithium-Ion Cells Series Battery Pack in Electric Vehicles. *J. power sources* 242, 699–713. doi:10.1016/j.jpowsour.2013.05.071

Xiong, R., Sun, F., He, H., and Nguyen, T. D. (2013). A Data-Driven Adaptive State of Charge and Power Capability Joint Estimator of Lithium-Ion Polymer Battery Used in Electric Vehicles. *Energy* 63, 295–308. doi:10.1016/j.energy.2013.10.027

Xue-min, S., and Deng, L. (1997). "Game Theory Approach to Discrete H∞ Filter Design," in IEEE Transactions on Signal Processing (IEEE), 1092–1095. doi:10.1109/78.564201

Yang, N., Zhang, X., and Li, G. (2015). State of Charge Estimation for Pulse Discharge of a LiFePO4 Battery by a Revised Ah Counting. *Electrochimica Acta* 151, 63–71. doi:10.1016/j.electacta.2014.11.011

Zhang, F., Liu, G., Fang, L., and Wang, H. (2012). "Estimation of Battery State of Charge with H-Infinity Observer: Applied to a Robot for Inspecting Power Transmission Lines," in IEEE Transactions on Industrial Electronics (IEEE). doi:10.1109/TIE.2011.2159691

Zhang, X-M., and Han, Q-L. (2008). Robust H∞ Filtering for a Class of Uncertain Linear Systems with Time-Varying Delay. *Automatica* 44, 157–166. doi:10.1016/j.automatica.2007.04.024

Zhou, Y., Zhang, C., Zhang, Y., and Zhang, J. (2015). A New Adaptive Square-Root Unscented Kalman Filter for Nonlinear Systems with Additive Noise. *Int. J. Aerosp. Eng.* 2015, 381478. doi:10.1155/2015/381478

Conflict of Interest: The authors declare that the research was conducted in the absence of any commercial or financial relationships that could be construed as a potential conflict of interest.

Publisher's Note: All claims expressed in this article are solely those of the authors and do not necessarily represent those of their affiliated organizations, or those of the publisher, the editors, and the reviewers. Any product that may be evaluated in this article, or claim that may be made by its manufacturer, is not guaranteed or endorsed by the publisher.